ETH
Eidgenössische Technische Hochschule Zürich
Swiss Federal Institute of Technology Zurich

Empa
Materials Science and Technology

Semester Project

Thermal Simulation of Laser Powder Bed Fusion Process: Single Tracks

Andrea Kossinna

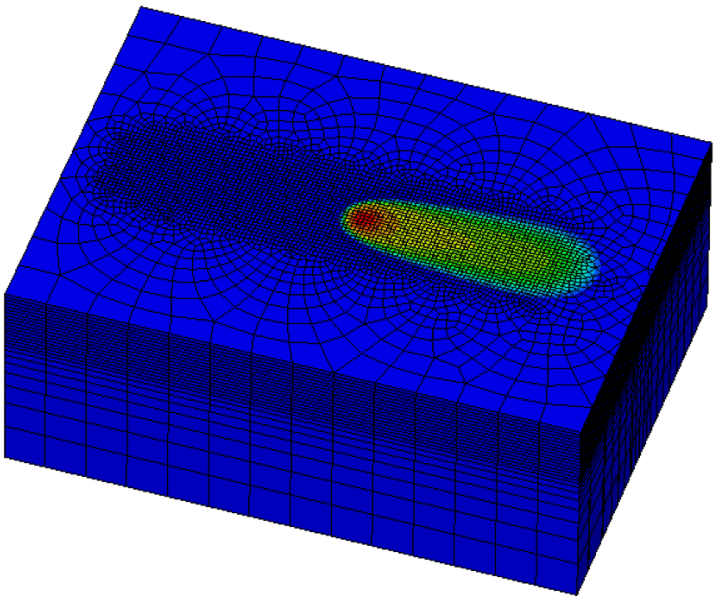

Advisors: Prof. Dr. E. Mazza, Dr. E. Hosseini, P. Gh Ghanbari

Experimental Continuum Mechanics Lab, EMPA
Department of Mechanical Engineering, ETH Zürich

Spring 2021

Abstract

Additive manufacturing is a promising production process with many advantages, e.g. be able to manufacture complex lightweight structures, which was not possible with conventional processes. In order to reach industrial standards, it is necessary to optimize the process parameters such as the laser power, scanning speed, powder layer thickness, hatch spacing, preheating temperature, scanning patterns, etc. This is usually done through an experimental trial and error approach. In order to save costs and resources, there is plenty of ongoing research on numerical simulations of the laser powder bed fusion (LPBF) process. The inclusion of all physical phenomena occurring at the micro-scale would lead to a complex and computational costly model. Therefore, some modelling assumptions and simplifications are made. This work evaluates the predicted melt pool shape of a simple thermal finite element model by comparing the simulation results with experimental data of Hastelloy X single track samples. The model assumptions are questioned and a sensitivity analysis is performed with respect to the input parameters. This work gives insight into the parameter interaction and their importance on the predicted result.

Acknowledgments

Firstly, I would like to thank Prof. Edoardo Mazza for giving me the opportunity to do this semester project at the Experimental Continuum Mechanics Lab and providing all the resources. I would like to express my sincere gratitude to my supervisor Dr. Ehsan Hosseini and my advisor Pooriya Gh Ghanbari, for their continuous support, patience, motivation, help with the programming and in-depth knowledge. I am also very grateful to Jian Tang, who helped me with the post processing of the simulation data, and the other team members who shared their expertise with me. Finally, I would like to thank my parents and Viviane Wolfer for their encouragement and proofreading my thesis.

Eidgenössische Technische Hochschule Zürich
Swiss Federal Institute of Technology Zurich

Declaration of originality

The signed declaration of originality is a component of every semester paper, Bachelor's thesis, Master's thesis and any other degree paper undertaken during the course of studies, including the respective electronic versions.

Lecturers may also require a declaration of originality for other written papers compiled for their courses.

I hereby confirm that I am the sole author of the written work here enclosed and that I have compiled it in my own words. Parts excepted are corrections of form and content by the supervisor.

Title of work (in block letters):

THERMAL SIMULATION OF LASER POWDER BED FUSION PROCESS: SINGLE TRACKS

Authored by (in block letters):

For papers written by groups the names of all authors are required.

Name(s):	**First name(s):**
KOSSINNA	ANDREA

With my signature I confirm that

- I have committed none of the forms of plagiarism described in the 'Citation etiquette' information sheet.
- I have documented all methods, data and processes truthfully.
- I have not manipulated any data.
- I have mentioned all persons who were significant facilitators of the work.

I am aware that the work may be screened electronically for plagiarism.

Place, date	**Signature(s)**
13.06.2021	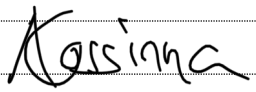

For papers written by groups the names of all authors are required. Their signatures collectively guarantee the entire content of the written paper.

Contents

1 Introduction

The laser powder bed fusion process (LPBF) or selective laser melting process (SLM) offers many advantages such as almost no design limitations. While originally, additive manufacturing methods were only used for rapid prototyping, the quality of SLM has improved significantly over the past two decades, making them suitable for the production of high quality products [1]. Today, there are many applications in marine, biomedical equipment and fuel cell [2]. Nevertheless, there are still some difficulties to face like porosity defects and residual stresses, which cause distortion and failure of the final parts [3]. In order to reach industrial standards, it is necessary to optimize the process parameters such as laser power, scanning speed, powder layer thickness, hatch spacing, preheating temperature, scanning patterns, etc. As their interplay is not fully understood an experimental trial and error approach to investigate the optimal parameters is very costly and time consuming [4]. For that reason numerical simulations of the LPBF process are done to find optimal process parameters. Unfortunately, the computational effort of these simulations is still very high and needs further improvement for industrial usage.
This thesis proposes a thermal model which predicts the melt pool dimensions of single track samples by performing simulations using commercially available finite element software. The sensitivity of the model with respect to its input parameters is investigated and analysed to identify general trends between the SLM process parameters and the melt pool size. For the validation of the model the predicted melt pool dimensions are compared with published single track experiments done on Hastelloy X at Waterloo University [5].

1.1 Selective Laser Melting Process

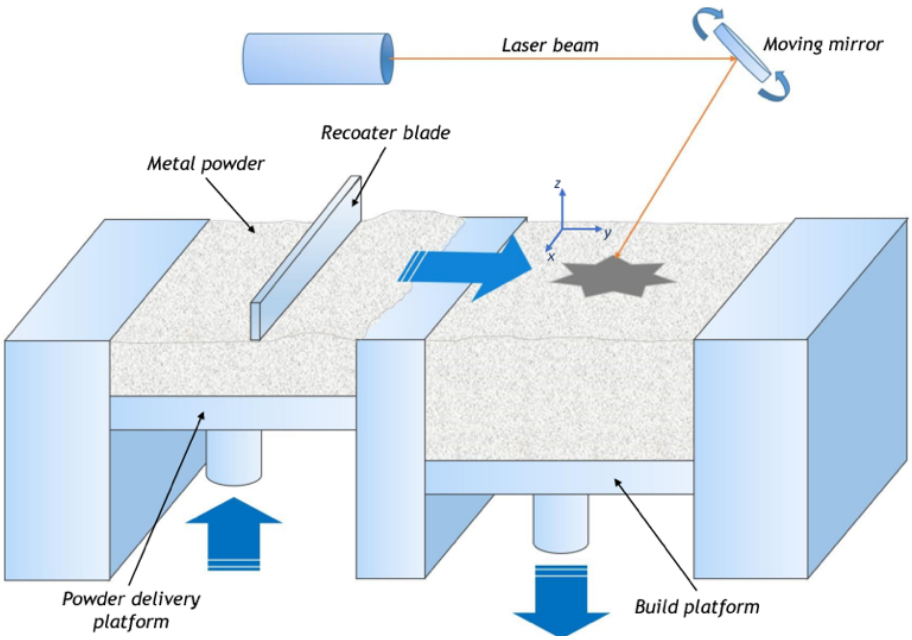

Figure 1: Illustration of the selective laser melting process [1]

In the selective laser melting process, contrary to conventional (subtractive) manufacturing process, the parts are additively manufactured, which means in a layer-upon-layer manner [1]. A thin layer of powder, typically 20–50 microns, is spread by a recoater blade over the build platform. The laser, which is focused and directed to the correct location, scans the build platform, locally

fusing the powder particles to create a layer of the part. Afterwards, the build platform is lowered by the depth of the powder layer thickness and a new layer of powder is distributed evenly across the platform. These steps are repeated until the whole geometry is fabricated. The process takes place in a non-oxidative environment maintained by nitrogen or argon gas, while the temperature of the build chamber might be increased using attached heaters. Any excess powder after the recoating is gathered in a storage container and can be reused [6].

1.2 Influence of Process Parameters

It has been extensively reported for many materials that the melt pool depth increases with increasing laser power and decreases with increasing scanning speed [7]. Using a higher scan speed will lead to a higher fabrication rate and the melt pool becomes longer. At a very high scan speed the time is not sufficient for the heat to diffuse across the whole powder bed, which could lead to insufficient melting and ablation of the powder [6]. Another disadvantage is that high scan speeds can lead to discontinuity, meaning a longer melt pool breaks into shorter melt pools [6, 7]. Furthermore, a high scan speed also requires high laser power to maintain the required laser energy density for melting [2], which means higher costs [1]. Moreover, high power inputs are considered only suitable for materials with high thermal conductivities like aluminium and copper, because spattering will occur if the input heat is not dissipated fast enough [2]. On the other hand, with a low scan speed the porosity increases as keyhole pores are formed as vapor bubbles are trapped within the melt pool [8]. Therefore, the scan speed needs to be chosen carefully, see Figure 2.

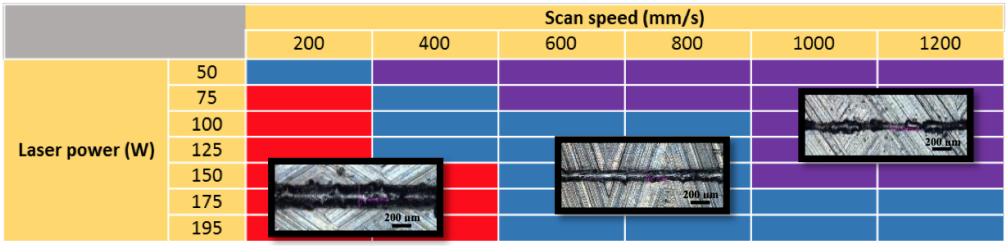

Figure 2: Results of Ti-6Al-4V single track experiments at different scan speed and laser powers with constant (30µm) powder layer thickness; red zone: vaporization induced porosity, blue zone: good melt pool characteristics, purple zone: unstable melt pools [9]

Form other studies of single tracks experiments it is reported that the most influencing parameter is the laser power and then, in order of decreasing importance, the powder layer thickness, the scanning speed, and finally the particle size [10].
Moreover, a smaller layer thickness leads to better accuracy of the manufactured part, and also better remelting of the previous layer thus providing stronger bond between the layers. On the other hand, it increases the manufacturing time. When choosing the thickness of a layer, it is also necessary to consider the particle size and shrinkage during melting [6].

2 Modelling

Since it is difficult to take all the physical phenomena occurring in the LPBF process into account, computational models are based on assumptions that may neglect or simplify some physics of the process. It would be necessary to include fluid dynamics to model convective effects such as for example the Maragoni convection, which is caused by the surface tension gradient resulting from thermal gradients in the free melt surface [11]. Unfortunately, this inclusion would result in high computational effort and more complexity. In this section it is explained which common assumptions are made to simulate the LPBF process for an acceptable computational effort and which input parameters of the process are highly disputed. Further, the different heat source models are discussed.

2.1 Uncertainty in the Laser Absorption Parameter

In the LPBF process some parameters are very difficult to determine as they either depend on multiple factors or are difficult to measure. The following fish-bone diagram gives an overview of the factors influencing the thermal aspects of the LPBF process.

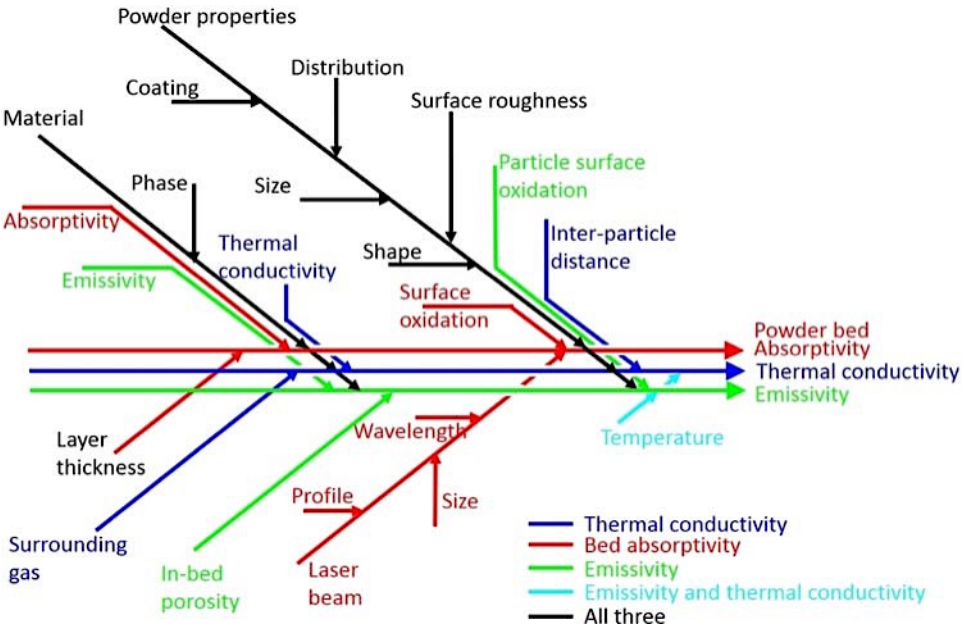

Figure 3: Uncertainty sources for thermal analysis of LPBF process according to Moges et al. [12]

When a laser beam hits a substrate only a fraction of the deposited energy is absorbed by the material and the rest is reflected. The absorptivity is therefore defined as the ratio of optical power absorbed by the material to the incident power applied [13]. As seen in the fish-bone diagram the absorptivity or laser absorption efficiency in the SLM process depends on several factors such as beam intensity, wavelength, polarization, powder material properties like size, shape, distribution, and porosity, oxidation etc [12, 11]. For materials with a flat surface, the absorptivity can be extracted from the reflectivity measurements. But for powder, the absorptivity measurement is difficult as high angle scattering is important [13]. Additionally, thermal radiation from the heated sample complicates the measurements. It was demonstrated that, due to multiple scattering, the powder absorptivity is greatly increased in comparison to flat surface absorptivity [4, 13, 14]. There are numerical approaches to predict the absorptivity of powder, for example the proposed

ray tracing model from Boley et al. [15]. For experimental measurements either an integrating sphere is added to the reflectivity measurement to collect as much of the reflecting light as possible and calculate the powder absorptivity [13]. Another option is a calorimetric approach, where a thin powder layer in a metal disk is exposed to a uniform light source and the absorptivity is calculated from the temperature increase, measured by thermocouples [13]. In their study [13], using the calorimetric approach, they found no significant absoptivity change in the temperature range between 20-500°C, suggesting therefore no strong temperature dependency. Further, they measured approximate absorptivity values, 70% for Ti-6Al-4V, 65% for stainless steel, and 57% for aluminium. Similar calorimetric measurements were done by Trapp et al. [14] to investigate the relationship between the laser power and the absorptivity of a flat 316L stainless steel plate. They found that after an apparent critical power threshold a sharp increase in absorptivity is seen from 30% to 70% and a saturation at 78%. Comparing that with the melt pool shape, this drastic increase coincides with the formation of a keyhole. It was explained that in the keyhole mode multiple light scattering on the keyhole walls enhances the light absorption. Moreover, absorptivity measurements on a substrate covered with a 100-µm powder layer had shown a two times higher absorptivity compared to substrate only. With increasing laser power the absorptivity showed a similar increase as the absorptivity of the flat plate [14]. As the absorptivity between powder and bulk material differs a lot, it might be reasonable to assign field variables to the absorptivity and the heat source model, as the absorptibity is included in the heat source model. An other option is to consider the absorptivity as a function of the powder layer thickness, where at decreasing powder thickness the absorptivity slowly approaches the absorptivity value of bulk material. However, in literature mostly a constant value for the absorptivity is taken and found to be sufficient [11, 3]. Some papers also suggest a temperature dependent laser absorptivity [13]. Shahabad et al. [16] consider the absorptivity as being proportional to the laser power and inversely proportional to the square root of the scan speed ($\frac{P}{\sqrt{V}}$), because at an increasing energy density, the melt pool depth becomes larger due to higher heat penetration of the powder bed [16]. These authors refer to the absorbed energy density calculation by [17]. However, this is relationship is not found elsewhere in the literature. Nevertheless, considering the absorption as function of laser power and scan speed would be worth to investigate further.

2.2 Modeling the Powder Bed

There are two different approaches to model the powder bed. One of them is the powder-scale modeling approach, which considers the geometry, size, and distribution of the powder particles, the other one is the continuum-scale approach, which is based on the assumption of a continuum powder layer with effective thermo-physical properties [11]. The second approach has been widely adopted in the literature due to the lower computational effort compared to the powder-scale modeling, which, however, offers higher accuracy on a micro-scale level.

2.3 Heat Source Modelling

Where material parameters, geometries and other parameters are clearly defined, the modeling of the heat source provides many options. The heat source models are highly discussed as they directly influence the geometry of the melt pool, which on the other hand affects the microstructure and the mechanical performance of the final part. As the laser absorption efficiency is part

of the heat source model, multiple heat source models have been developed assuming various absorptivity values. Based on [3], the heat source models can be classified into two groups (see Figure 4): The geometrically modified group including cylindrical shape (a), semi-spherical shape (b), semi-ellipsoidal shape (c), conical shape (d), and the absorptivity profile group (e) containing the radiation transfer method, ray-tracing method, linearly decaying method, and exponentially decaying method. Nearly all the heat source models assume a two dimensional Gaussian heat distribution. The difference lies in the distribution of energy along the depth [18]. When the heat source is moving along the scanning track, the powder ahead of the laser beam is continuously melted and solidified behind the laser beam. Therefore, the heat flux is a function of space and time, which is termed as Gaussian moving heat source.

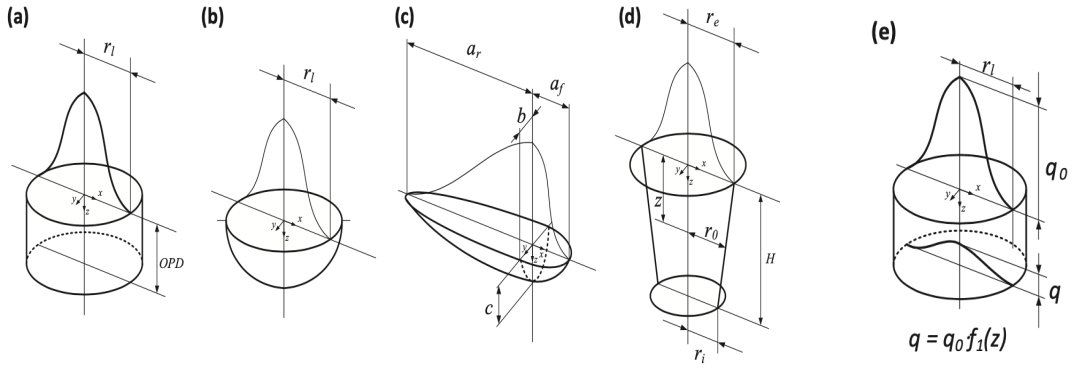

Figure 4: Different existing heat source models [3]

Generally, the distribution of heat flux can be described [18] :

$$q(r) = q_{max} exp(kr^2)$$

Where q_{max} is the maximum heat flux, k is concentration factor and r the distance between a point and center of the heat source. The maximum heat flux q_{max} can be obtained by integrating the heat flux over the whole area. Thus, the total thermal heat equals to the effective laser power Q [18], In the q_{max} the absorptivity of the powder material, the laser power and the maximum radius of laser spot is included. Goldak et al. [19] introduced the 3D double-ellipsoidal moving heat source, see Figure 4(c), as a first approach for the 3D heat source, and developed a FE model to investigate the thermal history in a welding application [11]. This heat source consists of two elliptic regions, one in the front of the arc centre, where x $>$ 0, and the other one behind the arc centre, x $<$ 0. The heat source can be written as;

$$q_{f,r}(x,y,z) = \frac{f_{f,r} 6\sqrt{3} Q}{a_{f,r} bc\pi^{\frac{3}{2}}} \exp\{-\frac{3(x-v_x t)^2}{a_{f,r}^2} - \frac{3(y)^2}{b^2} - \frac{3z^2}{c^2}\}$$

Bruna-Rosso et al. firstly implemented this semi-ellipsoid heat source model in the LPBF simulation and the model showed good agreement with the experimental results [3]. However, the difficulty of all the 3D heat source models is that they require a reasonable estimation of the penetration depth, which is in turn influenced by various factors such as material type, powder size, and geometry [11].

3 Methods

In this chapter it is explained how the model in Abaqus was set up, which parameter values were chosen and which assumption were made. Furthermore, the procedure of the sensitivity analysis is described and it is explained how the data is post processed and evaluated.

3.1 Experimental Data

To validate the simulation results, the experimental data of Hastelloy X samples were used, which has been collected by the university of Waterloo [5, 16]. The design of experiments for single line tracks consisted of different laser powers (from 150 W to 300 W) and scanning speeds (from 600 mm/s to 2000 mm/s). The laser power and velocity were selected based on different LED (Laser energy density). Six single laser scans (two per layer thickness) were applied on top of the 3D printed substrates (using default settings) to form single tracks of 25 mm length. The cross-section of the samples were polished and etched to measure the melt pool dimensions under the microscope.

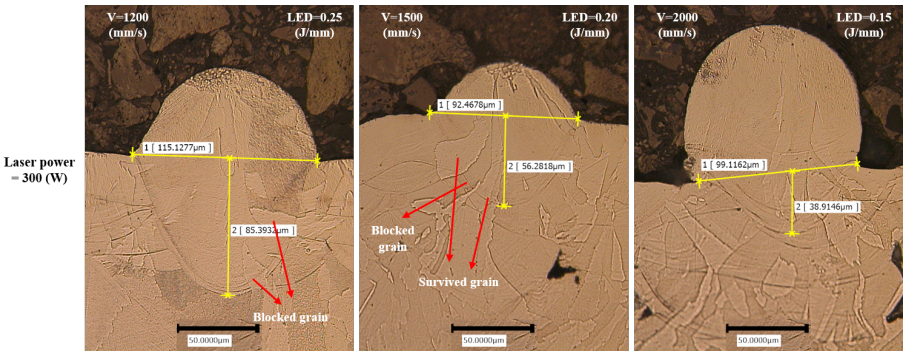

Figure 5: Micrograph of the melt pool at constant power and increasing scan speed [5]

They concluded that an increase in scanning speed has less influence on the melt pool size compared to a proportional increase in laser power. Moreover, they observed that the melt pool width is wider than the laser beam spot size (80 µm) due to the heat diffusion from molten metal to solid material [5]. Further, they reported almost no difference in melt pool depth between samples having a different powder layer thicknesses.

3.2 Modeling Assumptions

This thesis proceeds a FEM-based only thermal modelling approach, as the focus is on the melt pool dimensions which mainly depend on the temperature field. For simplicity, the fluid dynamics of the melt pool and all associated effects are ignored. As usual for simple SLM simulations, a continuum powder bed is assumed and the influence of the powder particle distribution neglected. As a heat source model, see Section 2.3, the Goldak model was chosen mainly because of its simple implementation. A mixture between the semi-spherical and semi-ellipsoidal where chosen by assuming that the heat source is rotationally symmetric in z-direction. Therefore, the Goldak parameter a_r, a_f and b are set equal. With this assumptions the number of free parameter was reduced from four to two. The parameter b is approximately the radius of the laser beam size.

3.3 Model Setup in Abaqus

For the simulations the commercial finite element Software Abaqus was used. Its advantage is that with the Additive Manufacturing Plug-in a moving heat source and especially the Goldak heat source model can be implemented easily. To keep the computation time as low as possible, the mesh was only refined where it was necessary namely in the range of the expected melt pool, and the laser is just moving up to the middle and not travelling the whole length of 1.4 mm. This builds on the assumption of having reached the steady state after a fixed time of $5 \cdot 10^{-4}$ s and the melt pool dimensions would not change anymore just changing position. From previous master thesis at Empa [20], a mesh optimization was done and the result was adopted here. But still the calculation time on the ETH Euler cluster with 12 cpus was around 3h. In Figure 6, it can be seen that a field variable was implemented to assign different material properties depending on the material state: 1 is for solid, 0 for powder. For numerical reasons it was linearly interpolated in-between.

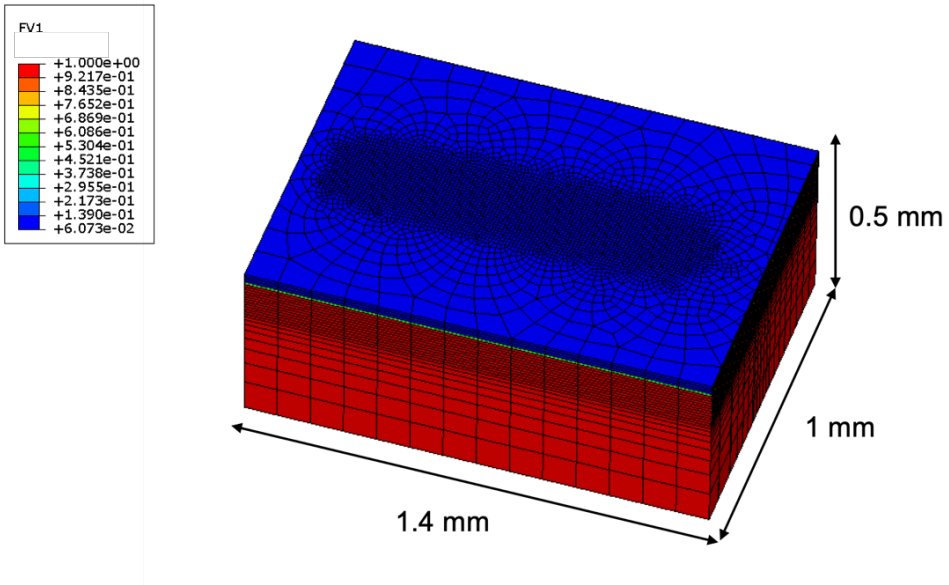

Figure 6: Abaqus model with assigned field variables

3.4 Process Parameters of SLM

The scan speed, laser power, laser spot size and powder layer thickness were chosen according to the experimental data from [5]. The temperature-dependent material properties of Hastelloy X for thermal conductivity, density, heat capacity and latent heat were taken from literature [16, 21]. The latent heat of fusion is the enthalpy needed to change the substrate from solid to liquid at constant pressure, meaning the energy required to break the bonds between the molecules [22]. In contrast to pure materials where the phase change takes place isothermal at a fixed melting temperature, the phase change of alloys typically happens gradually, meaning the latent heat is absorbed or released within a temperature interval between solidus temperature and liquidus temperature. To include the latent heat effects in LPBF models, there are two widely used schemes: the apparent heat capacity approach and the more involved heat integration method [23]. In this model the apparent capacity method is used. Therefore the heat capacity is modified in the melting range of Hastelloy X 1260°C-1355°C with the latent heat of 276 kJ/kg [24].

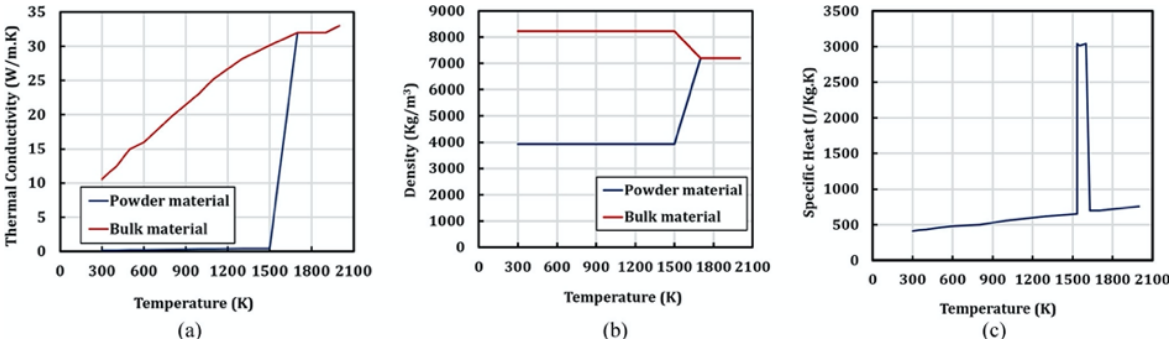

Figure 7: Material properties of powder and solid Hastelloy X [16]

To assign good values to the unknown heat source parameters and the uncertain laser absorption coefficient, a sensitivity analysis was performed in a first step, see Section 3.5. For the absorption coefficient of Hastelloy X a starting value of 60% was chosen, which is in the same range as the ones of other metal powders, see section 2.1.

3.5 Procedure of the Sensitivity Analysis

As the influence of the parameters and their interplay is not fully understood, this is investigated in the sensitivity analysis. The purpose of the sensitivity analysis is to point out the dominant parameters of the model, to then be able to investigate the influence of the laser power and scan speed to the melt pool dimensions. Therefore, the laser power, scan speed and powder layer thickness were fixed for this analysis. The laser power was set to 200W, the speed to 1000 mm/s and the layer thickness to 40µm, because this parameter set lies in the middle of the all parameter settings described in the data from Waterloo University [5]. Some further simulations were done at a second calibration point at 300W, 2000 mm/s and 60µm powder layer. In the sensitivity analysis only one of the investigated parameter was changed at the same time, while the others were set to the initial value. Therefore, the change in melt pool dimensions can be directly assigned to the change in the respective parameter. In Table 1 a list with the parameters is shown, which has been chosen according to their uncertainty and interest, which are mainly the heat source related ones and some powder related material properties that are difficult to measure.

Table 1: List of investigated parameters with assigned values

Parameter	initial value	changes
laser power absorption efficiency	65%	35, 50, 80, 95%
heat source parameter b	50 µm	35, 40, 60, 70 µm
heat source parameter c	100 µm	50, 75, 125, 150 µm
base-plate temperature	25°C	50, 100, 200°C
powder layer thickness	40 µm	20, 60 µm
heat capacity of material powder	0.124 W/(m*K) at 25°C 0.169 W/(m*K) at 1260°C	±25%
heat capacity of liquid material	544 W/(m*K) at 1660°C	±25%

As seen in Table 1 for the heat source parameters, more combinations were tested, as there was less knowledge present. As only one parameter is change at the same time the proposed changes lead to a total of 20 simulation runs for this sensitivity analysis, which means about 60 computation hours. Due to the large interest in the absorption, the sensitivity of a broad spectrum was analysed, starting from absorption values similar to bulk material (35%) to values (80%) which can be only justified in the keyhole formation zone (but as seen in the Figure 5 this is not the case) and up to quite unrealistic ones (95%) as a boundary.

3.6 Calculation of the Melt Pool

The output of the thermal simulation is the temperature at every node at each time step. To distinguish between melted and solid area a threshold value was set to the melting temperature of Hastelloy X T=1260°C. To have a continuous surface boundary between the melted and solid area, the data was linearly interpolated between the nodes of the mesh. The melt pool dimensions maximum depth, maximum width and maximum length can now be extracted from the melted area.

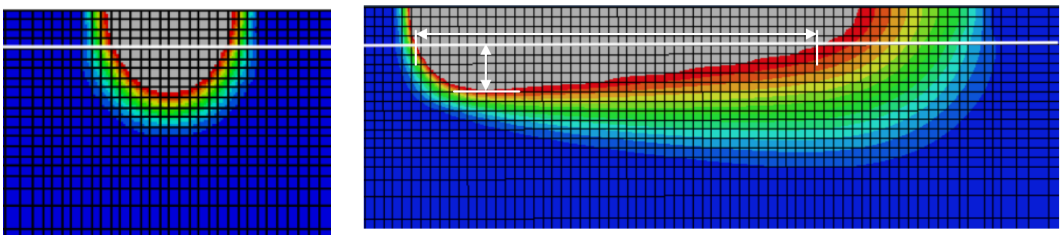

(a) Front view (b) Side view

Figure 8: Melt pool dimensions of a sample with a powder layer of 40 µm

To compare the simulation results with the experimental data it is important to be consistent in the melt pool definition. In Figure 5 of the experimental data it is seen that the melt depth was calculated as how much of the substrate was melted by the laser. The melted powder material, which is mainly forming the bead, was not included in the measurements. Therefore, in the post processing of the simulations, the melt pool was calculated starting below the powder layer as shown in Figure 8.

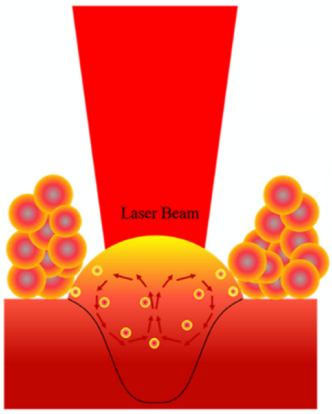

Figure 9: Schematic representation of the melt pool shape [5]

It is important to highlight that the simulated melt pool shape differs from the real one. Comparing

Figure 8(a) to Figure 9, the edge between powder, solid and melted material is sharp in the simulation while in reality it is smoother. A reason for these differences between the simulation and reality is that in the thermal simulation all dynamic effects were neglected and therefore also the fluid and material flow. In reality, the fluid flow would transfers more heat to this edge, meaning that the predicted width might be slightly smaller.

4 Results

In the following chapter the results of more than 30 evaluated simulations are presented, starting with the result and conclusion of the sensitivity analysis. Afterwards, the relationship between the laser scan speed and the melt pool dimensions is reported and thirdly, the influence of change in powder layer thickness on the predicted melt pool is analysed.

4.1 Sensitivity Analysis of the Model

The sensitivity analysis is an important part in understanding the heat source model and tuning the parameters for the comparison with the experimental data. In this section, the influence of each investigated parameter is shown and in a second step, they are compared to each other. All figures show the results using the calibration point (P=200W, v=1000 mm/s, t=40µm). The results from the second calibration point (P=300 W, v=2000 mm/s, t=60µm) is qualitatively mentioned in the text and the dashed lines in the figures represent the experimental values with this process parameters.

4.1.1 Heat Source Related Parameters

As mentioned, the Goldak heat source with the symmetrical assumption has been implemented in the simulation, see Sections 2.3 and 3.2. With increasing Goldak parameter c, the melt pool becomes deeper, thinner and shorter while the maximum temperature decreases. As expected, the melt pool depth is more affected (in percent) by this change than the melt pool width (in percent). As shown in the figure, the Goldak parameter c has to be increased tremendously to predict the experimental results accurately, as the resulting depth is nearly half of the heat source model depth. At the same time, the melt pool width decreases, therefore, the optimal value for c with respect to the width and depth lies around 130 µm.

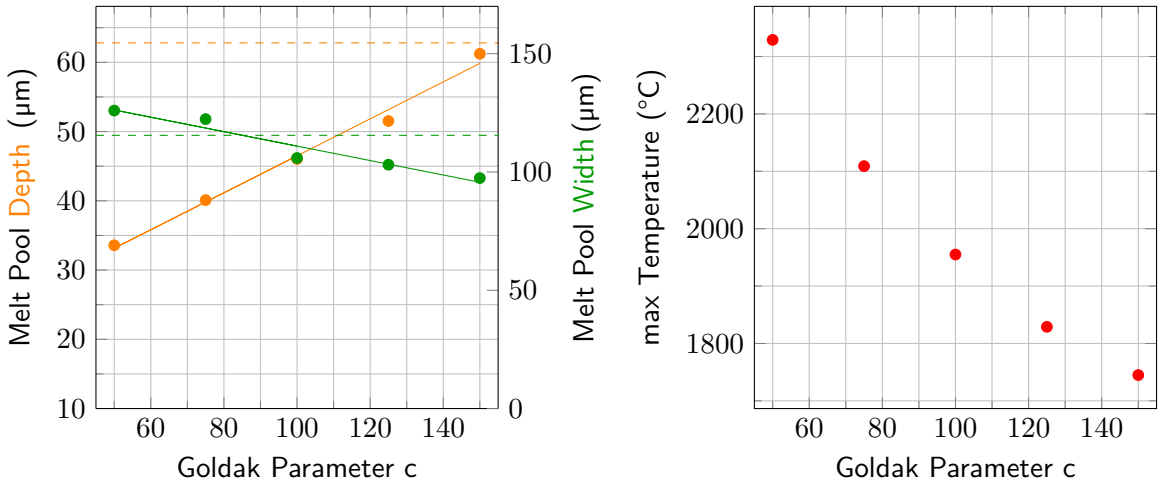

Figure 10: Influence of the heat source parameter c

In Figure 10 it is shown that a higher Goldak parameter b leads to a shallower and shorter melt pool while the maximum temperature decreases. Interestingly, the melt pool width is barely affected by a change of the heat source width b, but the melt pool depth decreases slowly. The change in melt pool depth can be explained with the constant laser power in the system, because

with a decreasing Goldak parameter b, the same amount of energy is assigned to a smaller area resulting in a deeper melt pool. However, the constant melt pool width can not be explained and, compared with Figure 10, the Goldak depth parameter c has a higher impact on the melt pool width than the Goldak width parameter b.

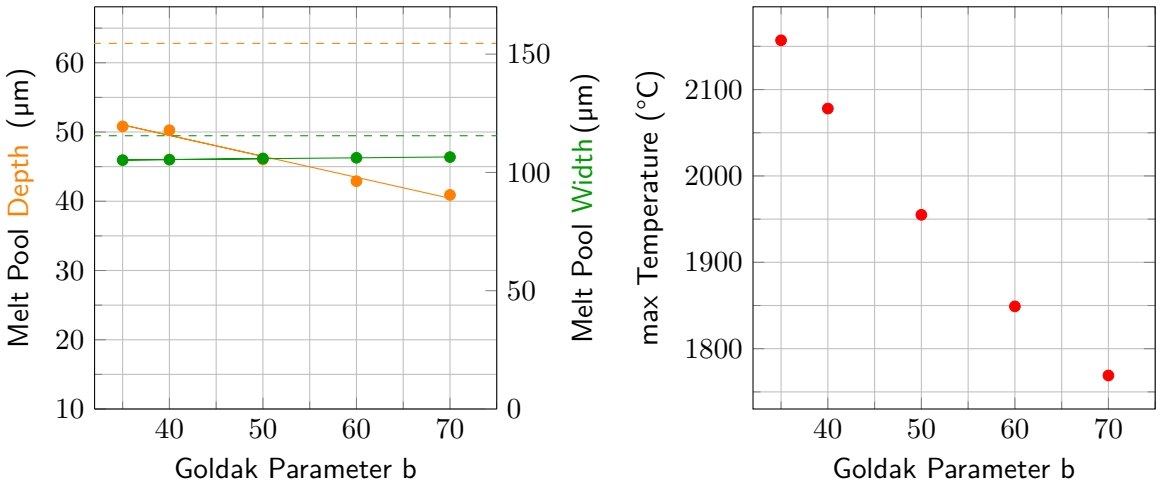

Figure 11: Influence of the heat source parameter b

As a remark, a simulation on welding, which used the Goldak double ellipsoid heat source model, also reported a decrease of the melt pool depth and the peak temperature with increasing parameter b [25]. But their set up differs and the dimensions are one order of magnitude higher. Both heat source parameters showed the same behaviour of the maximum temperature, whereas the smallest values of the parameter c reaches the highest temperature. This temperature behaviour can be again related to the constant energy source, as the volume (width and depth) of the modeled heat becomes larger, the energy is distributed over a bigger volume and therefore the maximum temperature decreases. The sensitivity analysis at the second calibration point showed the same result; with an increase in c the depth increases and the width only decreases slightly and with an increase in b the depth decreases and the width is nearly unaffected.

4.1.2 Laser Absorption Efficiency

As mentioned above, the laser absorption efficiency value is highly disputed. Therefore, the sensitivity of this model to the absorption efficiency was investigated and the results are presented in Figure 12. With an increasing absorption efficiency, the melt pool becomes deeper, thicker and much longer, as there is more energy taken up from the laser. From the results a linear relationship between the absorption efficiency and the melt pool width and depth could be assumed, where the melt pool width is more sensitive to the change and therefore shows a larger slope. However, the curve of the melt pool length vs absorption efficiency increases steeply from 185 µm at 35% to 420 µm at 65% and flattens between 80% and 95%. The maximum temperature increases with a higher absorption value, which was expected as more energy were taken up. The experimental width could be predicted with a absorption value of 70% but to reach the experimental depth a highly unrealistic value would be needed.

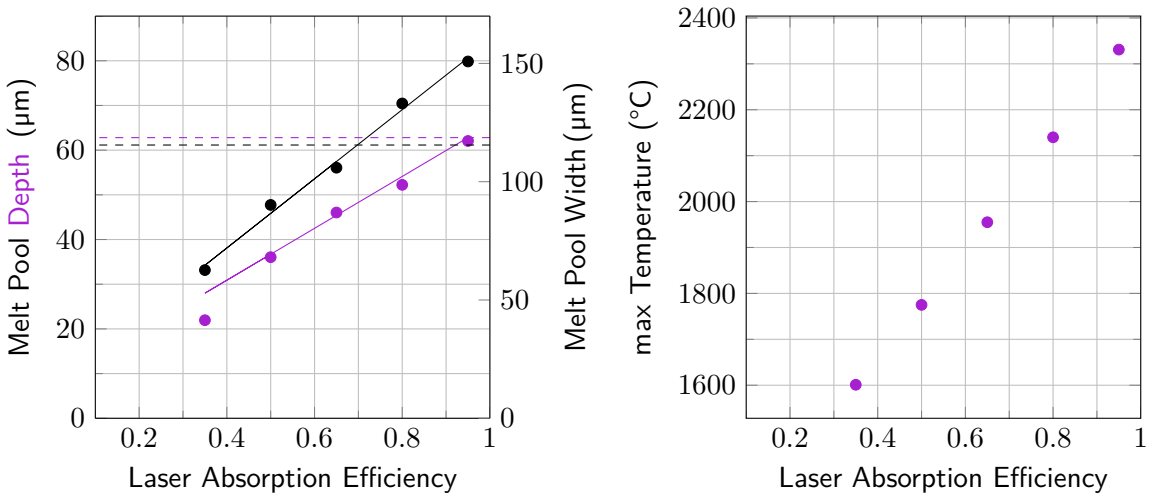

Figure 12: Influence of the laser absorption efficiency

The sensitivity analysis at the second calibration point showed that a change in the absorption value effects the melt pool length the most, then the depth and the width. This slightly different order could be explained by the higher powder layer thickness and the resulting melt pool shape at deeper level at the second calibration point, see Figure 18.

4.1.3 Base Plate Temperature

The base plate temperature of the experiments is not clearly mentioned but assumed to be at room temperature. Therefore, some investigation was done regarding this parameter. With an increasing base plate temperature, the melt pool becomes deeper, thicker and longer. Although, the base plat temperature has been increased to 200°C the max Temperature only increases by 20°C.

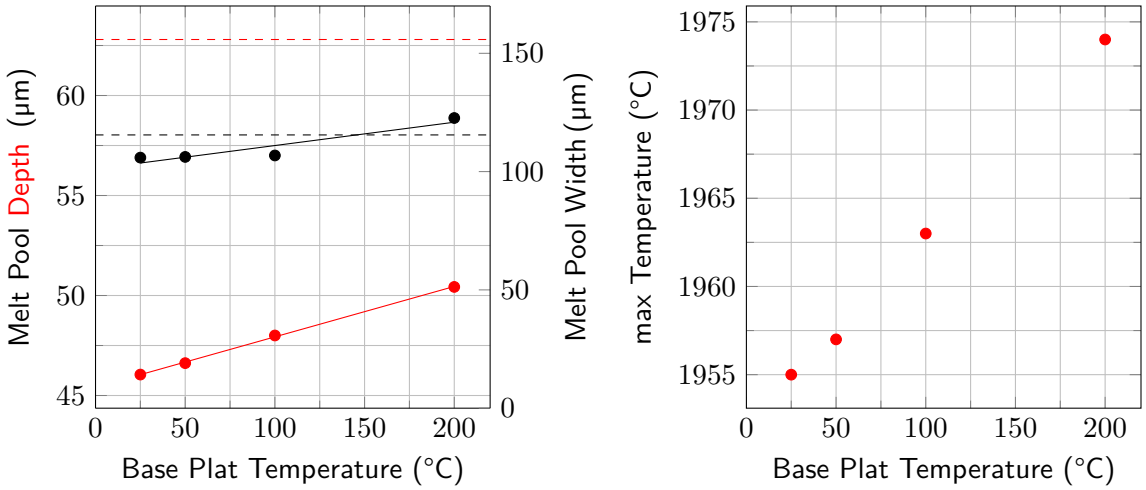

Figure 13: Influence of the base plate temperature

4.1.4 Heat Capacity of the Material

The heat capacity of the material powder shows a certain error compared to the solid material. Therefore, it was investigated how an uncertainty of ±25% influences the result. The initial values of the powder heat capacity were 124 at 25°C and 169 at 1260°C. Surprisingly, all simulation provided exactly the same result. Also at second calibration point the change in the heat capacity of the powder is not seen in the melt pool dimensions either. In a next step the heat capacity of the liquid material was changed as seen in Figure 14.

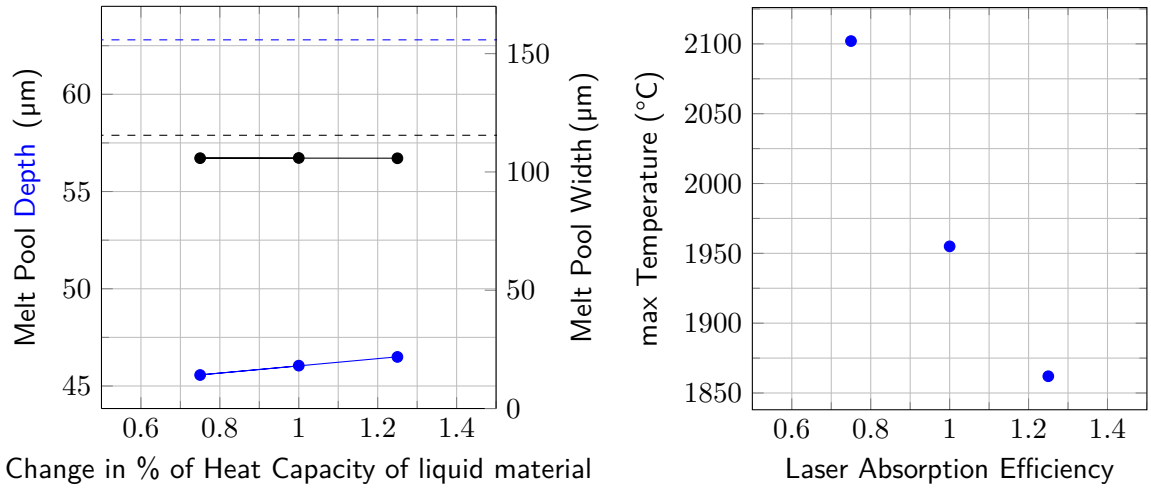

Figure 14: Influence of the heat capacity in the liquid state

With an increasing heat capacity, the melt pool becomes a little deeper and shorter, while the maximum temperature decreases sharply. The heat capacity is defined as the amount of heat supplied to a given mass of a material to produce a unit change in its temperature. Because the amount of heat from the laser stays constant and the heat capacity is increased, the change in temperature has to be smaller.

4.1.5 Conclusion of the Sensitivity Analysis

To draw a conclusion, the different parameters have been compared to each other. For that purpose each parameter was first increased by 25% and then by 50% of the initial value. The resulting melt pool dimensions and maximum temperature were normalised with respect to their initial result to have the change in percentage. In the following spider diagram it is shown that the the model is not sensitive to a small variation in the thermal conductivity of the powder or liquid material. Concluding the model is robust to possible errors in those quantities. The melt pool width is mostly influenced by the laser absorption efficiency, by a 25% increase of the absorption value, the melt pool width enlarges to 125%. The melt pool depth is mostly influenced by the Goldak parameter c, by a 25% increased c value, the melt pool width enlarges to 117%.

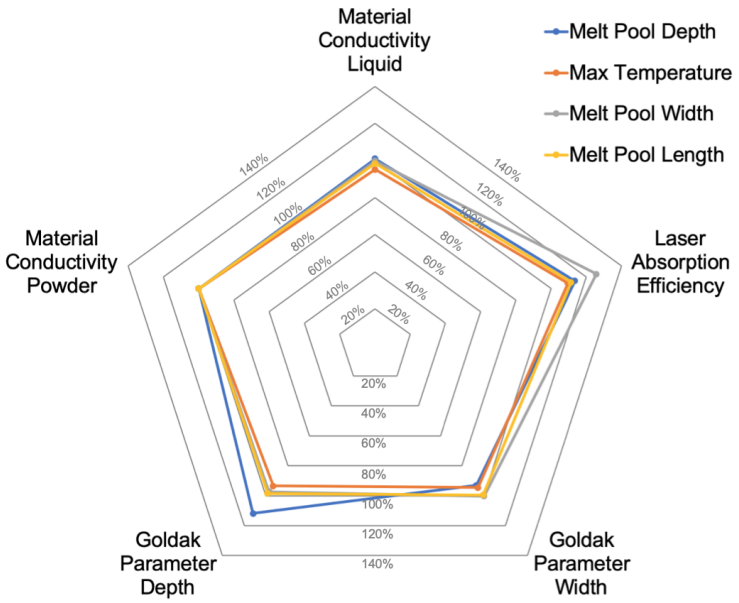

Figure 15: What happens to the calculated melt pool size when the respective parameter is increased by 25% ?

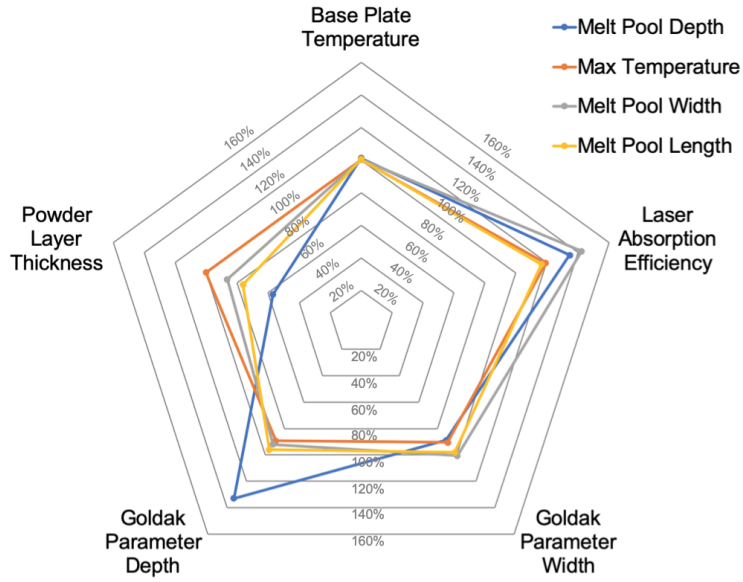

Figure 16: What happens to the calculated melt pool size when the respective parameter is increased by 50%?

In Figure 16, it is shown that the base plate temperature has a very low impact on the result compared to the other parameters. On the contrary, the powder layer thickness has a huge influence on all dimensions and reduces the melt pool depth by a significant amount. It is important to know the laser absorption efficiency influences all quantities, while the Goldak depth could be used to tune mostly the melt pool depth of the model.

Another finding of this investigation is that in general no correlation was found between the maximum temperature and one of the melt pool dimensions. The assumption of steady state after $5 \cdot 10^{-4}$ s is valid, as the maximum occurring temperature is already settled after a time of $3 \cdot 10^{-4}$ s and from then no difference in the simulation result was seen.

4.2 Comparison Simulation Result vs. Experimental Data

After the sensitivity analysis, the melt pool dimensions were predicted according to the experimental input parameters. The simulation were performed for three different scan speeds and for three different powder layer thicknesses at constant laser power (200 W). For the comparison, the absorption efficiency was kept at 65%, which is already at the upper limit, as it is not in the keyhole mode.

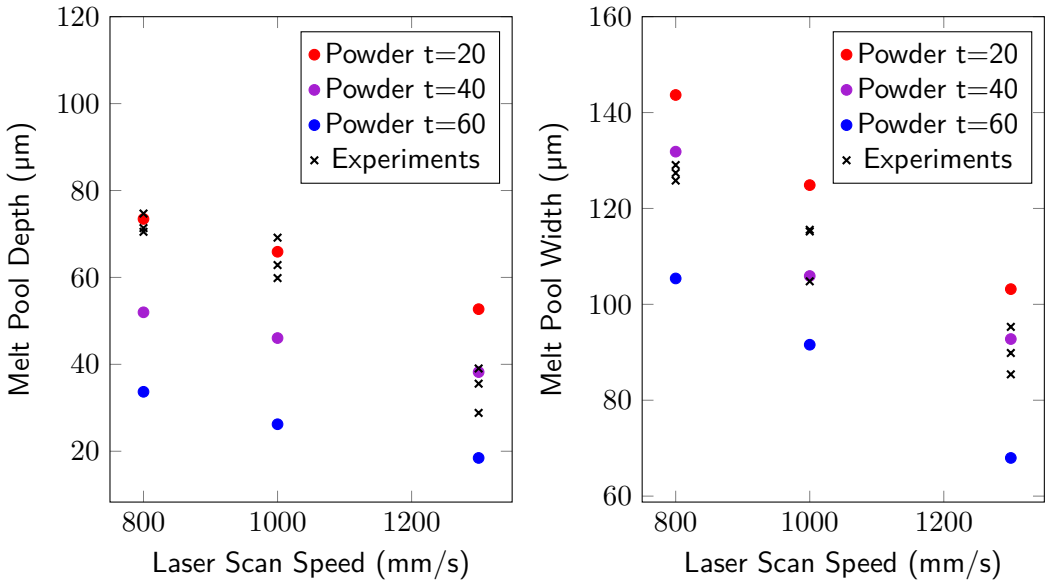

Figure 17: Experimental data vs. predicted melt pool dimensions for different scan speeds

The figures show that only the predicted melt pool depth at a powder layer thickness of 20 µm is close to the experimental data and the prediction of 40 µm is the closest for the melt pool width. In contrast to the experiments, where barely no difference with increasing powder thickness can be seen, the model is very sensitive to the powder layer thickness. At this point, it is important to mention that in the experiments the surface of the printed substrate was not polished or measured. Therefore, the effective layer thickness from former layers might be dominant in terms of controlling the melt pool geometry and the variation of nominal layer thickness (from 20 to 60 m) for the last layer deposition would be insignificant [16]. Thus, for further research it would be important to ensure a flat surface to validate the sensitivity of the powder thickness on this simulation. Another weakness of the experimental data plotted in the figure is that the two measurements of the same single track differ on average about 9.3 µm which leads to a high standard deviation of 13.8 m. For the comparison of simulation result with the experimental data the average was taken. The high standard deviation can be explained with the uncertainty in the powder layer along the build direction. Therefore, the experimental data could not be used to validate the model and no conclusion of the model accuracy can be done.

However, the max temperature does not differ between the different powder thicknesses and is at every scan speed within 7 degrees. The temperature decreases from 2019°C at 800 mm/s to 1868°C at 1300 mm/s. Additionally, the change of the melt pool shape was analysed, see Figure 18.

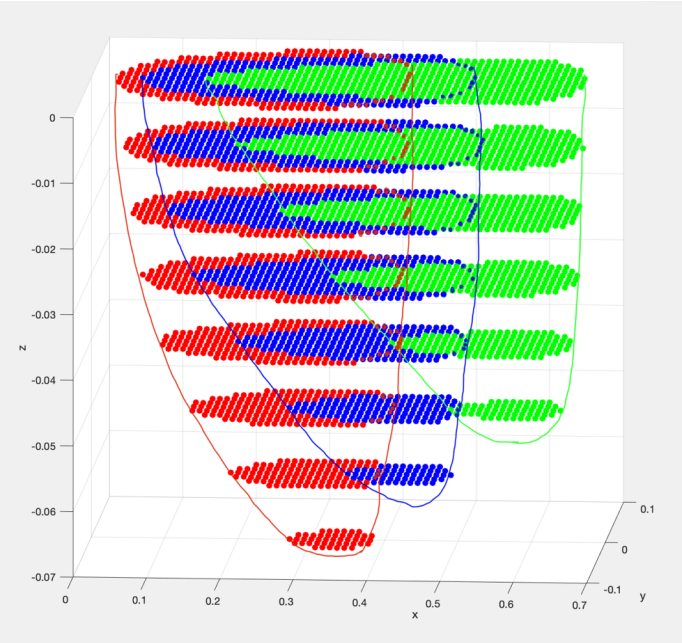

Figure 18: Shape of the melt pool with increasing scan speed (powder layer t =20 µm)

With increasing scan speed the the melt pool shape is elongated and the melt pool depth decreases. At a higher speed the melt pool length decreases fast along the depth whereas for a slower scan speed the melt pool length decreases more slowly along the depth, showing a more parabolic melt pool shape. Hence, it is important at which z-plane the melt pool length is measured. In Figure 18 the powder layer is between z=0.02 mm and z=0. The melt pool length at the z=0 plane clearly increases with an increasing scan speed. But the melt pool prediction with a 60µm powder layer would be similar to the melt pool at z=-0.04 mm in this figure. Therefore, it can be concluded that the melt pool length decreases with increasing speed, which is due to the change in the melt pool shape.

4.3 Uniformed Heat Source Model

As the Abaqus AM plug-in offers also a simple implementation for the uniformed heat source model, one simulation was performed to get an impression of the predicted melt pool dimensions resulting from another heat source model. Instead of having the Goldak parameters, three box lengths, one in each direction, can be chosen. All other parameters are the same as those from the initial settings of the sensitivity analysis.

Table 2: Comparison between the Goldak heat source model and the uniform heat source model

	[µm]	[µm]	[µm]	depth [µm]	width [µm]	length [µm]	max. T [°C]
Goldak	a_r, a_f=50	b=a_r=50	c=100	46	106	421	1955
Uniform	l_x=50	l_y=50	l_z=100	21	67	191	1693

Surprisingly, the predicted melt pool using the uniformed heat source model differs a lot from the predicted melt pool using the Goldak heat source model. Especially, the melt pool length is not even half of the melt pool predicted with the Goldak model. The uniformed heat source model has a different heat decaying coefficient which might explain those results. Further the volume of the

box is larger than the volume of the semi-ellipse with the same characteristic values. Therefore, the heat is assigned to a larger area. For deeper understanding, further simulations should be performed with the uniformed heat source model.

5 Conclusion

In this work the importance of the heat source parameters, the powder layer thickness and the layer absorption efficiency has been shown, resulting from the performed sensitivity analysis. The base plate temperature and the heat capacity of powder and liquid material barely showed any influence on the melt pool dimensions. Therefore, the efforts to determine those values exactly can be reduced. The sensitivity analysis at both calibration points qualitatively showed the same result. In general, there was no correlation seen between the maximum temperature and the melt pool dimensions. However, it might be of interest to further investigate this in an experimental setup.

Although the model parameters were investigated and tuned, it was not possible to predict the experimental values. The model could not be validated with the given experimental data set. Still, the results predicted with the smallest powder layer thickness were close to the experimental data. However, to validate the model, it would be necessary to perform the experiments in our own lab to have full control of all parameters and have as little uncertainty as possible. To investigate the impact of the powder layer thickness, the surface roughness of the substrate should be measured before printing the single track to avoid a high variation of the powder thickness itself. Moreover, multiple measurements of the same single track should be done to have a lower standard deviation of the melt pool dimensions as in the discussed experimental data set. For the model validation additional experiments and simulations using a different material than Hastelloy X are recommended.

For future work, it would be necessary to clarify the highly disputed energy absorption value and maybe consider the energy absorption efficiency as a function of scan speed, laser power and powder layer thickness, whereas in this work the absorption efficiency was kept constant. Moreover, it would be interesting to compare the predicted melt pool dimensions resulting from different heat source models. For example, investigate the difference between the Goldak heat source model with our proposed symmetrical assumption with the conical heat source shape, which was used in [16].

As a conclusion, the thermal finite element model predicted reasonable results and is convenient to extract the melt pool shape. It was noticed that the computational effort can even be reduced without losing accuracy by decreasing the time, which the laser travels in the simulation, by 40%. If this thermal model could be validated with accurate experimental data, the parameter settings could be transferred to a thermo-mechanical model for the prediction of residual stresses.

List of Figures

List of Tables

Bibliography

[1] Valeriya Griffiths, James P. Scanlan, Murat H. Eres, Antonio Martinez-Sykora, and Phani Chinchapatnam. Cost-driven build orientation and bin packing of parts in selective laser melting (slm). *European Journal of Operational Research*, 273(1):334–352, 2019.

[2] Zhongji Sun, Xipeng Tan, Shu Beng Tor, and Wai Yee Yeong. Selective laser melting of stainless steel 316l with low porosity and high build rates. *Materials Design*, 104:197–204, 2016.

[3] Zhidong Zhang, Yuze Huang, Adhitan Rani Kasinathan, Shahriar Imani Shahabad, Usman Ali, Yahya Mahmoodkhani, and Ehsan Toyserkani. 3-dimensional heat transfer modeling for laser powder-bed fusion additive manufacturing with volumetric heat sources based on varied thermal conductivity and absorptivity. *Optics Laser Technology*, 109:297–312, 2019.

[4] Saad A. Khairallah and Andy Anderson. Mesoscopic simulation model of selective laser melting of stainless steel powder. *Journal of Materials Processing Technology*, 214(11):2627–2636, 2014.

[5] Ali Keshavarzkermani, Ehsan Marzbanrad, Reza Esmaeilizadeh, Yahya Mahmoodkhani, Usman Ali, Pablo D. Enrique, Norman Y. Zhou, Ali Bonakdar, and Ehsan Toyserkani. An investigation into the effect of process parameters on melt pool geometry, cell spacing, and grain refinement during laser powder bed fusion. *Optics Laser Technology*, 116:83–91, 2019.

[6] Sanjay Kumar. *Additive Manufacturing Processes*. Springer, 2020.

[7] Valérie Gunenthiram, Patrice Peyre, Matthieu Schneider, Morgan Dal, Frédéric Coste, and Rémy Fabbro. Analysis of laser–melt pool–powder bed interaction during the selective laser melting of a stainless steel. *Journal of Laser Applications*, 29(2):022303, 2017.

[8] Subin Shrestha, Thomas Starr, and Kevin Chou. A study of keyhole porosity in selective laser melting: Single-track scanning with micro-ct analysis. *Journal of Manufacturing Science and Engineering*, 141:1, 04 2019.

[9] Haijun Gong, H. Gu, K. Zeng, J. S. Dilip, D. Pal, B. Stucker, D. Christiansen, and J. Lewandowski. Melt pool characterization for selective laser melting of ti-6al-4v pre-alloyed powder. 2014.

[10] Igor Yadroitsev, Ina Yadroitsava, Philippe Bertrand, and Igor Smurov. Factor analysis of selective laser melting process parameters and geometrical characteristics of synthesized single tracks. 18(3):201–208, 2021/03/25 2012.

[11] Kubra Karayagiz, Alaa Elwany, Gustavo Tapia, Brian Franco, Luke Johnson, Ji Ma, Ibrahim Karaman, and Raymundo Arróyave. Numerical and experimental analysis of heat distribution in the laser powder bed fusion of ti-6al-4v. *IISE Transactions*, 51(2):136–152, 2019.

[12] Tesfaye Moges, Gaurav Ameta, and Paul Witherell. A Review of Model Inaccuracy and Parameter Uncertainty in Laser Powder Bed Fusion Models and Simulations. *Journal of Manufacturing Science and Engineering*, 141(4), 02 2019. 040801.

[13] A. Rubenchik, S. Wu, S. Mitchell, I. Golosker, M. LeBlanc, and N. Peterson. Direct measurements of temperature-dependent laser absorptivity of metal powders. *Appl. Opt.*, 54(24):7230–7233, Aug 2015.

[14] Johannes Trapp, Alexander M. Rubenchik, Gabe Guss, and Manyalibo J. Matthews. In situ absorptivity measurements of metallic powders during laser powder-bed fusion additive manufacturing. *Applied Materials Today*, 9:341–349, 2017.

[15] C. D. Boley, S. A. Khairallah, and A. M. Rubenchik. Calculation of laser absorption by metal powders in additive manufacturing. *Appl. Opt.*, 54(9):2477–2482, Mar 2015.

[16] Shahriar Imani Shahabad, Zhidong Zhang, Ali Keshavarzkermani, Usman Ali, Yahya Mahmoodkhani, Reza Esmaeilizadeh, Ali Bonakdar, and Ehsan Toyserkani. Heat source model calibration for thermal analysis of laser powder-bed fusion. *The International Journal of Advanced Manufacturing Technology*, 106(7):3367–3379, 2020.

[17] Haniyeh Fayazfar, Mehrnaz Salarian, Allan Rogalsky, Dyuti Sarker, Paola Russo, Vlad Paserin, and Ehsan Toyserkani. A critical review of powder-based additive manufacturing of ferrous alloys: Process parameters, microstructure and mechanical properties. *Materials Design*, 144:98–128, 2018.

[18] Zhibo Luo and Yaoyao Zhao. A survey of finite element analysis of temperature and thermal stress fields in powder bed fusion additive manufacturing. *Additive Manufacturing*, 21:318–332, 2018.

[19] John Goldak, Aditya Chakravarti, and Malcolm Bibby. A new finite element model for welding heat sources. *Metallurgical Transactions B*, 15(2):299–305, 1984.

[20] N. Smatsi, Surrogate modeling for 3D multiscale thermal simulations of powder-bed additive manufacturing, Master Thesis, ETH Zürich and Empa, Zürich, Switzerland, 2020.

[21] HASTELLOY® X alloy. `http://haynesintl.com/docs/default-source/pdfs/new-alloy-brochures/high-temperature-alloys/brochures/x-brochure.pdf?sfvrsn=15b829d4_40`. Last visited: May 29, 2021.

[22] David R. Legates. *Latent Heat*, pages 450–451. Springer Netherlands, Dordrecht, 2005.

[23] Sebastian D. Proell, Wolfgang A. Wall, and Christoph Meier. On phase change and latent heat models in metal additive manufacturing process simulation. *Advanced Modeling and Simulation in Engineering Sciences*, 7(1):24, 2020.

[24] J. J. Valenica and P. N. Quested, Thermophysical properties, pp. 468–481. ASM Handbook Committee, 2008. `https://materialsdata.nist.gov/bitstream/handle/11115/166/Thermophysical%20Properties.pdf?sequence=3&isAllowed=y`. Last visited: June 11, 2021.

[25] John H. Chujutalli, Marcelo I. Lourenço, and Segen F. Estefen. Experimental-based methodology for the double ellipsoidal heat source parameters in welding simulations. *Marine Systems & Ocean Technology*, 15(2):110–123, 2020.